Article

Neoadjuvant anti-PD1 immunotherapy for surgically accessible recurrent glioblastoma: clinical and molecular outcomes of a stage 2 single-arm expansion cohort

Check for updates

A list of authors and their affiliations appears at the end of the paper

Glioblastoma is immunologically "cold" and resistant to single-agent immune-checkpoint inhibitors (ICI). Our previous study of neoadjuvant pembrolizumab in surgically-accessible recurrent glioblastoma identified a molecular signature of response to ICI and suggested that neoadjuvant pembrolizumab may improve survival. To increase the power of this observation, we enrolled an additional 25 patients with a primary endpoint of evaluating the cell cycle gene signature associated with neoadjuvant pembrolizumab and performed bulk-RNA seq on resected tumor tissue (NCT02852655). Neoadjuvant pembrolizumab was associated with suppression of cell cycle/cancer proliferation genes and upregulation of T-cell/interferon-related gene expression. This signature was unique to patients treated with neoadjuvant pembrolizumab and was an independent positive risk factor for survival. Our results demonstrate a clear pharmacodynamic effect of anti-PD1 therapy in glioblastoma and identify pathways that may mediate resistance. However, we did not confirm a survival benefit to neoadjuvant pembrolizumab in recurrent glioblastoma and our secondary endpoint of PFS-6 was 19.5% (95% CI: 9.29-41.2%) for the pooled neoadjuvant cohorts. Our new data suggests some patients may exhibit innate resistance to pre-surgical ICI and require other concomitant therapies to sensitize effectively.

Glioblastoma is the most aggressive primary brain cancer in adults and two-thirds of patients are inherently resistant to the current standard-of-care systemic therapies[1]. Despite the impressive intracranial activity of immune-checkpoint inhibitors (ICIs) in pathologies such as melanoma brain metastases, glioblastoma is resistant to single-agent immune-checkpoint blockade[2–5]. To better understand the molecular response of glioblastoma to ICIs and to identify targetable pathways of immune evasion, we previously reported on a pilot randomized surgical window-of-opportunity trial of neoadjuvant followed by adjuvant pembrolizumab versus adjuvant pembrolizumab alone in patients with recurrent glioblastoma

underdoing surgical resection[6]. Analysis of bulk gene expression profiles of neoadjuvant-pretreated versus untreated tumors uncovered a molecular response signature that consisted of downregulation of cell cycle/cancer proliferation genes and upregulation of T cell/interferon-γ -related genes. Cell cycle gene signatures were inversely correlated with overall survival. Importantly, the addition of neoadjuvant treatment with pembrolizumab was associated with a statistically significant increase in overall survival compared to treatment with adjuvant pembrolizumab alone. Here we report the results of a single-arm, non-randomized neoadjuvant pembrolizumab expansion cohort (NCT02852655) to increase the

e-mail: Patrick_Wen@dfci.harvard.edu

power of our pharmacodynamic endpoint, the tumor molecular response to pembrolizumab, and its effect on overall survival.

Results

To confirm the pharmacodynamic effects of pembrolizumab in glioblastoma, we designed an expansion cohort to our previously reported pilot, multicenter, randomized, open-label, surgical study of neoadjuvant plus adjuvant pembrolizumab (neoadjuvant arm) versus adjuvant pembrolizumab alone (adjuvant arm) in patients with recurrent glioblastoma undergoing surgical resection (Fig. 2A)[6]. All patients were allocated to the neoadjuvant arm and received a single dose of pembrolizumab approximately 14 days prior to surgical tumor resection followed by pembrolizumab every 3 weeks after surgical recovery until disease progression or unacceptable toxicity. A total of 25 patients were enrolled between June 2020 and August 2021 at four institutions and comprise the intention-to-treat population (SFig. 1 and STable 1).

In our initial investigation, pembrolizumab treatment resulted in a decrease in cell cycle/cancer proliferation gene signatures and increased T cell/interferon-γ signature. The cell cycle/cancer proliferation gene signature inversely correlated with survival[6]. The primary objective of the current expansion cohort was to increase the power of this observation and test the hypothesis that administration of pembrolizumab leads to a decrease in the expression of cell cycle/cancer proliferation-related gene signatures in the composite pooled cohorts (see clinical trial protocol, Appendix A).

We conducted gene expression analysis of resected tumor tissue in our expanded neoadjuvant cohort using bulk-RNA sequencing (RNAseq) and pooled it with the gene expression data from stage 1 of our clinical trial as a pre-planned primary endpoint for this expansion study (Fig. 1a). The clinical trial met its primary pharmacodynamic endpoint as composite gene expression analysis found a statistically significant decrease in the median cell cycle/cancer proliferation-related absolute enrichment score to −0.2996 (IQR −0.5853 to 0.2040) in pembrolizumab-treated tumor tissue in the neoadjuvant cohorts, compared to 0.5172 (IQR 0.0712-0.6579) in untreated tumor tissue from the adjuvant cohort (Fig. 1b, $p = 0.009$). Interestingly, the extent of cell cycle gene set downregulation was not as pronounced in the expansion cohort (SFig. 4A). Our pooled cohorts also showed a heterogenous enrichment of T cell/IFN gene signatures in pembrolizumab-treated tumor tissue compared to untreated (Fig. 1c, $p = 0.08$). Individual analysis of the two neoadjuvant cohorts also maintained the same pattern of gene expression changes in cell cycle and interferon-γ-related genes compared to the adjuvant cohort, though it did not reach significance for the expanded neoadjuvant cohort (SFig. 4A, B). As in our initial study, neoadjuvant pembrolizumab treatment did not induce a statistically significant increase in tumor-infiltrating lymphocytes relative to the adjuvant-only treated cohort (TIL, SFig. 5). These findings confirm a pharmacodynamic effect of PD1-directed ICIs on the gene expression patterns of glioblastoma but suggest the existence of mechanisms that may mediate innate resistance by preventing T cell infiltration or inhibiting TIL function in the TME, as we have recently shown[7].

In order to develop a biomarker that can inform about the clinical course of these patients, we used a Cox proportional hazard model to identify gene signatures differentially expressed in our neoadjuvant cohorts that were also independently associated with survival. The cell cycle gene signature (Farmers_Breast_Cancer_Cluster_2)[8] was downregulated by neoadjuvant pembrolizumab treatment and found to be an independent risk factor for overall survival (Fig. 1d, HR 3.54, CI [1.17–10.65], $p = 0.025$). Adding the cell cycle gene signature (Farmers_Breast_Cancer_Cluster_2)[8] to the Cox model substantially increased the explained variance in overall survival (i.e., the R squared)[9] from 32% to 45%, which is consistent with the findings in our initial report[6]. Interestingly, the interferon-γ-related gene set (Ayers_et_al_IFN_genes)[10] did not independently correlate with survival

(SFig. 4C, HR 0.93, CI [0.32-2.70], $p = 0.893$), suggesting that Type 1 and Type 2 interferons are difficult to distinguish and may represent chronic inflammation that mediates inherent resistance to ICI. Total steroid dose at registration was the only clinical factor significantly associated with survival along with cell cycle in this cohort (Fig. 1d, HR 1.44, CI [1.06–1.95], $p = 0.021$). Deconvolution of the bulk gene expression data using CybersortX showed that the change in cell cycle gene signature significantly and directly correlated with estimates of tumor fraction, while T cell/IFN_gene expression changes correlated with the myeloid fraction (Fig. 1e, f). These findings suggest that the suppression of cell cycle genes triggered by anti-PD1 immune-checkpoint blockade in glioblastoma bulk tumors is driven by tumor cells and independently linked with survival in these patients.

In the intention-to-treat analysis, median overall survival in the neoadjuvant expansion cohort was 204 days (6.8 months), compared to 417 days (13.7 months) in the initial neoadjuvant cohort and 228 days (7.5 months) in the initial adjuvant-only cohort. Median progression-free survival in the neoadjuvant expansion cohort was 75 days (2.5 months) compared to 99.5 days (3.3 months) in the initial neoadjuvant cohort and 72.5 days (2.5 months) in the initial adjuvant-only cohort, respectively (Fig. 2c). PFS-6 was 0% for the neoadjuvant expansion cohort, as opposed to 33.3% (95% CI: 16.3–68.2%) for our previously reported initial neoadjuvant cohort. Our secondary endpoint of PFS-6 for the pooled neoadjuvant cohorts was 19.5% (95% CI: 9.29–41.2%), compared to 13.3% (95% CI: 3.67–48.4%) in the adjuvant cohort. Median follow-up times are reported in Supplementary Table 4. There was no difference in overall or progression-free survival between the 3 cohorts ($p > 0.05$ and $p = 0.0543$, respectively, Mantel-Cox test). In patients that received surgery and had histologic evidence of recurrent glioblastoma (mITT), median overall survival was 209.5 days (7.0 months) for the neoadjuvant expansion cohort, compared to 400 days (13.2 months) in the initial neoadjuvant cohort and 192 days in the initial adjuvant-only cohort (Fig. 2b). The overall survival of patients in this expansion neoadjuvant cohort was modest compared to the initial neoadjuvant cohort in our randomized trial, but the pharmacodynamic endpoints suggest that the neoadjuvant dosing with pembrolizumab did not induce as much downregulation of tumor cell cycle genes as noted in the initial cohort (SFig. 4A).

To further evaluate the biological and clinical outcomes associated with these changes in gene expression, we classified patients into four groups based on their median cell cycle/cancer proliferation and T cell/interferon-γ-related gene signatures (Fig. 3a). Post-hoc analysis of survival times as a function of these signatures showed a significant difference in overall survival between the 4 groups (Fig. 3c, log-rank test, p value < 0.0001). Additionally, the proportion of neoadjuvant versus adjuvant patients varied significantly among the 4 quadrants (Fig. 3b, Chi-square test, $p = 0.027$). Interestingly, all patients in the subgroup with an interferon-high and cell cycle-low gene signature (Group 3) had received neoadjuvant pembrolizumab (13 out of 13 patients) and had significantly longer survival, 420 days (13.8 months), compared with the other subgroups (Fig. 3b, c). Survival for "cell cycle-low" groups was overall improved compared to "cell cycle-high" patients, which showed the lowest survival times (Groups 2 and 4). Isolating patients whose cell cycle and interferon signatures were both classified as high (Group 4) was associated with the lowest survival, with a hazard ratio for death of 7.46 (CI 1.22–45.46, p value = 0.029). Tumors with high interferon/T cell signatures had significantly higher TIL density compared to those with low interferon/T cell signatures (Fig. 3e, f). To investigate the biological processes that account for the large difference in survival between both interferon-high groups (Groups 3 and 4), we screened various inflammation/immune activation-related gene signatures. We found that Group 4 had differentially higher enrichment of STAT3 and TNF-α-related gene signatures compared with Group 3 (Fig. 3d). Aberrant activation of STAT3 and TNF-α has been related to tumor cell proliferation, invasion and
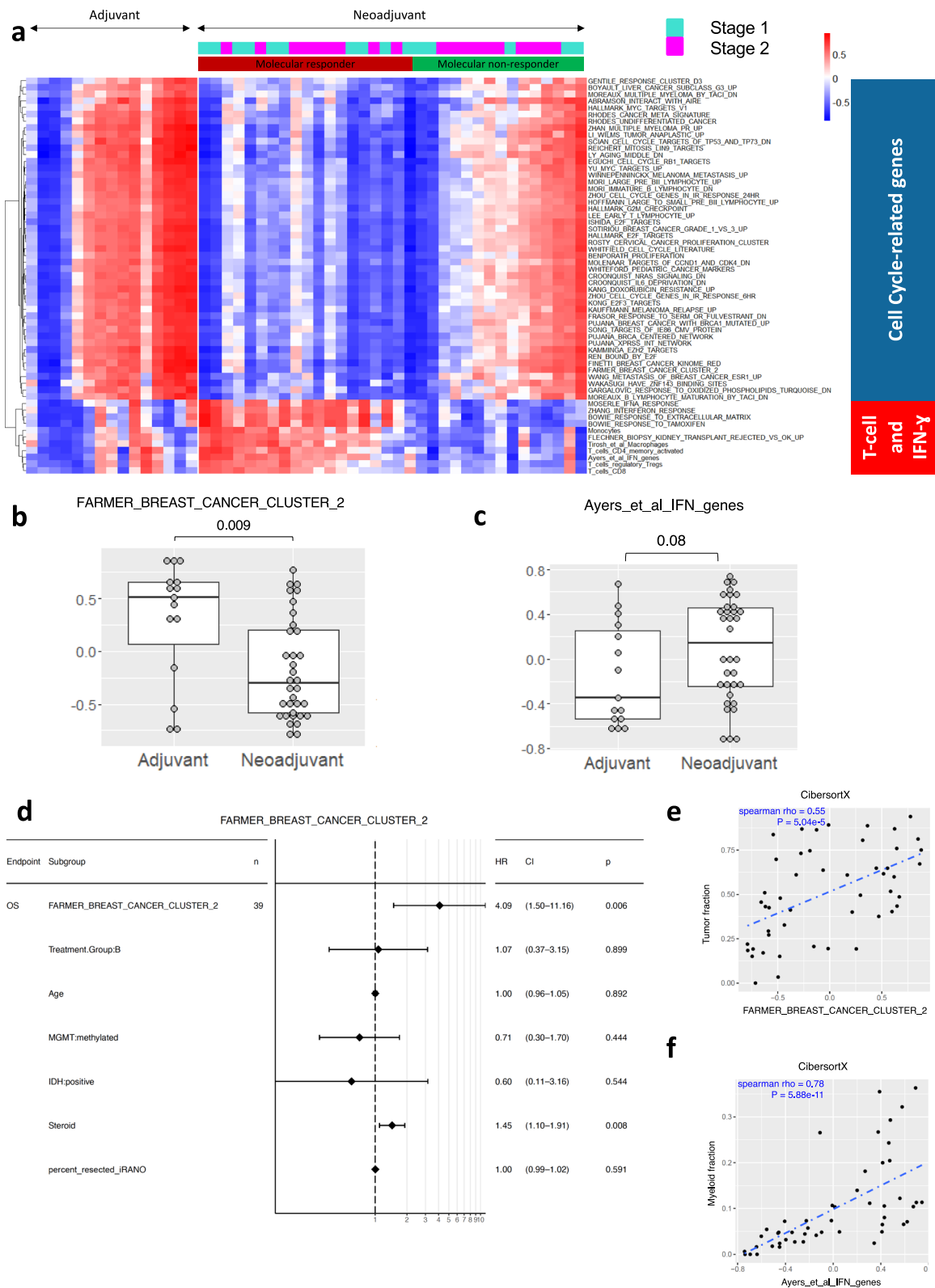
the recruitment of immunosuppressive cell populations such as MDSC and regulatory T cells[11]. Notably, STAT3 has been identified as a master regulator of the mesenchymal GBM subtype[12–14]. These findings suggest that neoadjuvant anti-PD1 immune-checkpoint blockade can trigger a change in tumor gene expression states to low cell cycle/cancer proliferation and high T cell/interferon-γ-related signatures, and that this expression profile is associated with T cell infiltration and the longest survival in this pembrolizumab-treated cohort.

The baseline characteristics of study participants are outlined in Supplementary Table 1. One patient was excluded from the modified intention-to-treat population (mITT) after analysis of resected tumor tissue failed to confirm recurrent glioblastoma (SFig. 1). Three patients were censored at day 1 for PFS by iRANO criteria due lack of follow-up

Fig. 1 | Pembrolizumab treatment is associated with increased T cell/interferon-γ-gene-related signatures and decreased cell cycle/cancer proliferation gene signatures. a Heat map of bulk tumor mRNA gene expression data showing gene signature analysis enrichment (GSAE) scores of gene sets with interquantile range ≥ 0.7. **b** Gene signature scores for Farmer_Breast_Cancer_Cluster_2 comparing pooled adjuvant and neoadjuvant cohorts. Each dot represents a patient, the lower and upper box bounds indicate the 25th and 75th percentile and the middle box line indicates the median value (adjuvant $n = 15$; neoadjuvant $n = 34$). P values were calculated using a two-sided Wilcoxon rank-sum test. **c** Gene signature scores for Ayers_et_al_IFN_genes comparing pooled adjuvant and neoadjuvant cohorts. Each dot represents a patient, the lower and upper box bounds indicate the 25th and 75th percentile and the middle box line indicates the median value (adjuvant $n = 15$; neoadjuvant $n = 34$). P values were calculated using a two-sided Wilcoxon

rank-sum test. **d** Forest plot of Cox proportional hazard model analyzing the effect of Farmer_Breast_Cancer_Cluster_2 and clinical variables on overall survival. Diamonds mark the hazard ratio (HR) estimates while error bars denote the 95% confidence interval (CI) of the HR. The P value of each covariate was based on its Wald statistics; the P values are not adjusted. **e** Correlation between tumor fraction as estimated by Cibersort X and Farmer_Breast_Cancer_Cluster_2 gene signature score. Each dot represents a patient ($n = 49$). The Spearman's rank correlation coefficient (ρ) and p value are calculated using a two-sided Spearman correlation test. **f** Correlation between myeloid fraction as estimated by Cibersort X and Ayers_et_al_IFN_genes gene signature score. Each dot represents a patient ($n = 49$). The Spearman's rank correlation coefficient (ρ) and p value are calculated using a two-sided Spearman correlation test. Source data are provided as a Source Data file.

scans. Baseline characteristics were similar between the initial and expanded neoadjuvant cohorts (STable 2). Pembrolizumab was well tolerated and this cohort did not uncover any new, unexpected toxicities. There were six CTCAE grade ≥3 events including cerebral edema (2), headache, fatigue, adrenal insufficiency and hyperthyroidism.

Discussion

Our expansion cohort of recurrent glioblastoma patients treated with neoadjuvant followed by adjuvant pembrolizumab met its primary pharmacodynamic endpoint. Our pooled gene expression analyses indicate a clear gene signature of pembrolizumab activity in recurrent glioblastoma that is associated with a decrease in cell cycle and cancer proliferation genes, and an increase in T cell/interferon-related genes. Prior studies have demonstrated that high baseline or on-treatment expression of interferon-γ in bulk tumor correlates with response to immune-checkpoint inhibitors[15,16]. Consistent with our initial report of a survival advantage to neoadjuvant pembrolizumab, we identify a subgroup of 13 patients specifically in our neoadjuvant cohort marked by high tumor interferon-γ signature and low cell cycle signature with very long survival at a median of 13.8 months. Similarly, analysis of baseline and on-treatment melanoma tumor samples from patients receiving immune-checkpoint inhibitors significantly correlated high interferon-γ signature accompanied by decreased G2M checkpoint genes to complete and partial clinical responses, suggesting these are broad biomarkers for benefit from immune-checkpoint blockade[17]. As interferon-γ induces cell cycle arrest in a number of cancer types, immune cell-derived interferon-γ may be directly responsible for the low cell cycle scores seen in our longest-surviving cohort[18,19].

The lowest survival group in our analyses consisted of patients with both high cell cycle/cancer proliferation genes and high interferon signature and was composed of patients in both the neoadjuvant and adjuvant cohorts of our clinical trial. Cancer is well recognized to produce a chronic inflammatory state. These data suggest that the local inflammatory response in the TME may be contextual because an equal fraction of patients (untreated vs. neoadjuvant) has evidence for high cell cycle and high T cell/IFN transcriptional signatures. Patients with this transcriptional pattern have tumors enriched in STAT-3 and TNF signaling. As such, these tumors may be similar to the mesenchymal subset of GBM[14,20] and suggest that this chronic inflammatory TME may be inherently resistant to ICI. Strategies to transiently reduce such chronic inflammation have had success in other extracranial tumor types[21], and subsequently restored responses to immune-checkpoint blockade[22–24].

Hyperactivation of the p16-CDK4/6-Rb signaling pathway, a major cell cycle regulator in glioblastoma, may also independently provide a mechanism for immune evasion. Cyclin-dependent kinases 4 and 6 signaling in both tumor and T cells has been previously implicated in mediating immune evasion through suppression of tumor-intrinsic antigen processing and presentation machinery, as well as through modulation of T cell subsets[25–29]. In melanoma, increased expression of CDK4 and E2F targets and decreased expression of class I HLA is

associated with resistance to anti-PD1 immunotherapy[29]. These findings led to significant interest in the combination of CDK4/6 inhibitors and immune-checkpoint inhibitors in tumors with frequent CDK4/6 hyperactivation, like glioblastoma[20]. Unfortunately, a phase 1b clinical trial of the CDK4/6 inhibitor abemaciclib in combination with the anti-PD1 antibody pembrolizumab in metastatic breast cancer revealed unacceptably high rates of severe transaminitis and interstitial lung disease (i.e., pneumonitis)[30]. For now, the question of whether targeting CDK4/6 signaling and immune checkpoints in combination results in significant anti-tumor activity remains unanswered.

The clinical impact of neoadjuvant immune-checkpoint blockade compared to adjuvant administration alone in recurrent glioblastoma remains unclear. We were unable to confirm a survival advantage of neoadjuvant pembrolizumab. Our neoadjuvantly treated expansion cohort had significantly lower survival than the neoadjuvant cohort of our initial randomized study. There was a trend for increased postoperative volumes and a higher proportion of IDH wild-type tumors in our expansion cohort compared to our initial neoadjuvant cohort which may have impacted survival, though they did not reach statistical significance. In melanoma, the SWOG S1801 trial demonstrated that neoadjuvant administration of immunotherapy significantly improves event-free survival in patients with stage III malignant melanoma compared to adjuvant immunotherapy alone despite equal number of immunotherapy treatments[31]. In these patients, pathologic response after 6–10 weeks of neoadjuvant therapy, defined as a pathologic assessment of resected tumor tissue showing 10% or less residual viable tumor, is the strongest indicator of benefit[31,32]. Although the more aggressive growth kinetics of glioblastoma do not allow for pathologic response assessments in those time-frames, our work highlights low cell cycle/cancer proliferation and high T cell/interferon-γ-related gene signatures as a potential early biomarker for response to immune-checkpoint blockade in recurrent glioblastoma that may serve as a basis for patient stratification in future clinical trials.

There are some important limitations to our study. It was not powered for survival analyses and the effect of neoadjuvant pembrolizumab on survival in recurrent glioblastoma remains unclear. Other limitations in our expansion cohort include its single-arm design, lack of a contemporaneous control cohort and small sample size. Future clinical trials should be powered for survival analyses and evaluate whether our biomarker signatures predict response to immune-checkpoint inhibition in glioblastoma.

Methods
Study design and patients
This study was approved by institutional review boards (IRB) at all sites (Dana-Farber Cancer Institute; Huntsman Cancer Institute; MD Anderson Cancer Center; Massachusetts General Hospital; Memorial Sloan Kettering Cancer Center; University of California, Los Angeles; University of California, San Francisco) and was conducted according to the Declaration of Helsinki. All patients provided written informed
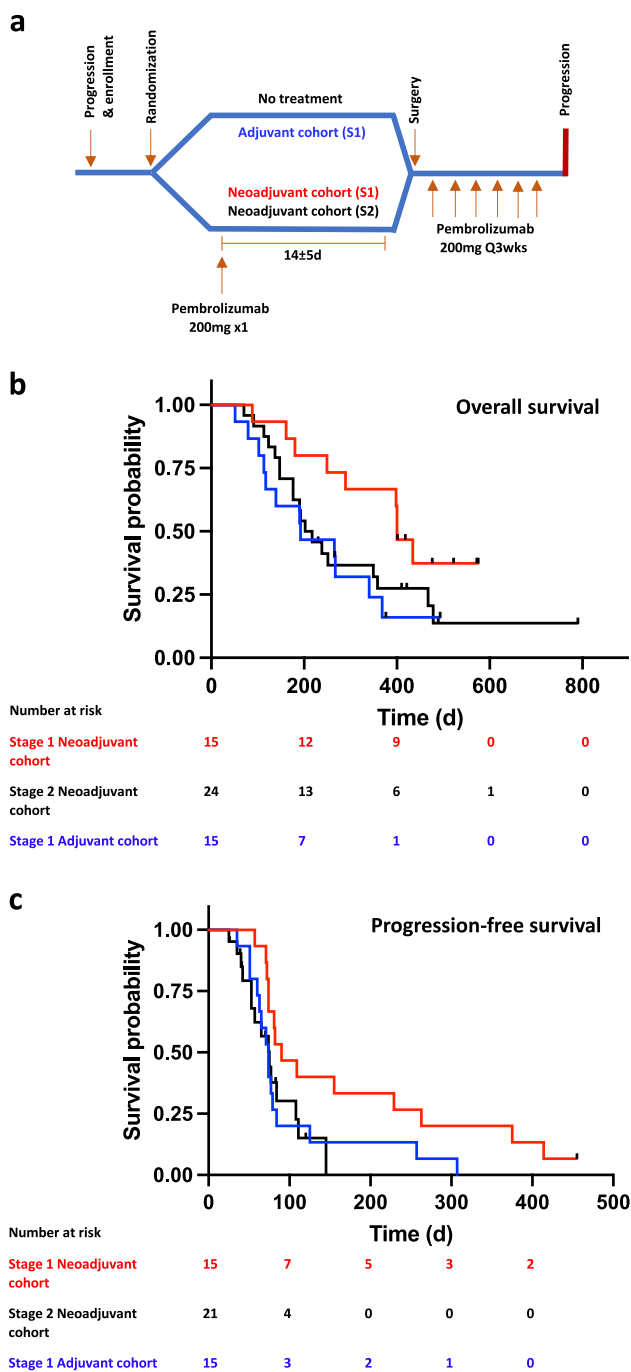
Fig. 2 | Clinical trial design and survival outcomes. Patients in the first stage of this clinical trial (S1) were randomized to no treatment prior to surgical resection of recurrent glioblastoma (Adjuvant cohort, S1, blue) or single dose of pembrolizumab 200 mg prior to surgery (Neoadjuvant cohort, S1, red). An additional 25 patients were enrolled in a second stage as a neoadjuvant expansion cohort (Neoadjuvant cohort, S2, black). **a** Clinical trial schema. **b** Kaplan–Meier plot of overall survival in the modified intention-to-treat population. Median survival of the neoadjuvant expansion cohort (black) was 209.5 days, compared to 400 days in the stage 1 neoadjuvant cohort (red) and 192 days in the stage 1 adjuvant cohort (blue) ($p = 0.0858$ logrank test). **c** Kaplan–Meier plot of progression-free survival in the modified intention-to-treat population. Median progression-free survival of the neoadjuvant expansion cohort (black) was 75 days, compared to 99.5 days in the stage 1 neoadjuvant cohort (red) and 72.5 days in the stage 1 adjuvant cohort (blue) ($p = 0.0543$ logrank test). Source data are provided as a Source Data file.

consent. Participants were not compensated. Eligibility criteria for the neoadjuvant expansion cohort were identical to the previous randomized trial. Patients were ≥18 years of age, had recurrent glioblastoma and were candidates for surgical debulking. Key eligibility criteria included Karnofsky performance status ≥70, previous first-line therapy with at least radiotherapy, first or second relapse with unequivocal evidence of tumor progression, adequate organ function, no high-dose systemic corticosteroids (defined as >4 mg day^{-1} of dexamethasone or bio-equivalent for at least three consecutive days within two weeks of registration) and absence of previous anti-angiogenic or antivascular endothelial growth factor agents. Sex of the participants was self-reported. The clinical trial is registered in clinicaltrials.gov under NCT02852655. The full study protocol is available under Supplementary Information as Appendix A.

After consent, patients enrolled into the neoadjuvant expansion cohort received pembrolizumab 200 mg by intravenous infusion 14 ± 5 d before scheduled surgical resection. Tumor resection was performed according to institutional standards. After recovery from surgery, patients received pembrolizumab 200 mg by intravenous infusion every 3 weeks until either tumor progression or an adverse event requiring study drug discontinuation. Blood samples were obtained every two cycles (6 weeks). Patients were followed for MRI changes, clinical exams and steroid doses until death or second progression. After second progression, patients were followed every 3 months for vital status until death.

Overall survival and progression-free survival were defined as time from date of registration to date of confirmed death or radiographic progression by iRANO criteria, respectively. Subjects without efficacy evaluation data or without survival data were censored at Day 1.

Tumor volume measurement

T1, T1C, FLAIR, and T2 MRI sequences for each study time point were preprocessed using automated tumor segmentation pipeline as described previously (https://www.ncbi.nlm.nih.gov/pmc/articles/PMC6051535/)(https://link.springer.com/chapter/10.1007/978-3-030-72087-2_20). Briefly, N4 bias field correction was applied to each sequence using the Insight Toolkit program (ITK, 2021, version 5.3.0; https://itk.org/) (https://pubmed.ncbi.nlm.nih.gov/15458157/)(https://pubmed.ncbi.nlm.nih.gov/32578020/). All sequences were resampled to 1 mm × 1 mm × 1 mm with linear interpolation and co-registered using the 3D Slicer program (3D Slicer, 2019, version 4.10.2; https://www.slicer.org/) (https://pubmed.ncbi.nlm.nih.gov/22770690/). Skull stripping was applied to the T1-weighted sequence using the Robust Brain Extraction program (ROBEX, 2013, version 1.2; https://www.nitrc.org/projects/robex/) (https://pubmed.ncbi.nlm.nih.gov/21880566/). Z-score pixel intensity normalization was applied to each MR sequence. DeepNeuro segmentation model was then applied to the four normalized and resampled images (https://www.ncbi.nlm.nih.gov/pmc/articles/PMC6051535/). The output label for enhancing tumor were then reviewed and manually edited, if needed, by a board-certified neuroradiologist (R.H., with 16 years of experience)using ITK-SNAP (ITK-SNAP, version 3.8.0; http://www.itksnap.org/pmwiki/pmwiki.php) (https://pubmed.ncbi.nlm.nih.gov/16545965/).

RNA and genomic DNA isolation

RNA and genomic DNA were extracted from resected tumor specimens preserved in AllProtect tissue reagent (Qiagen) at the time of surgery. For the initial cohort, we simultaneously isolated RNA and DNA using Qiagen AllPrep DNA/RNA kits (#80204). In the expanded cohort, we divided the tumor tissue in half and employed the Qiagen RNeasy Mini Kit (#74104) for RNA isolation and the Qiagen DNeasy Blood and Tissue Kit (#69504) for DNA isolation.
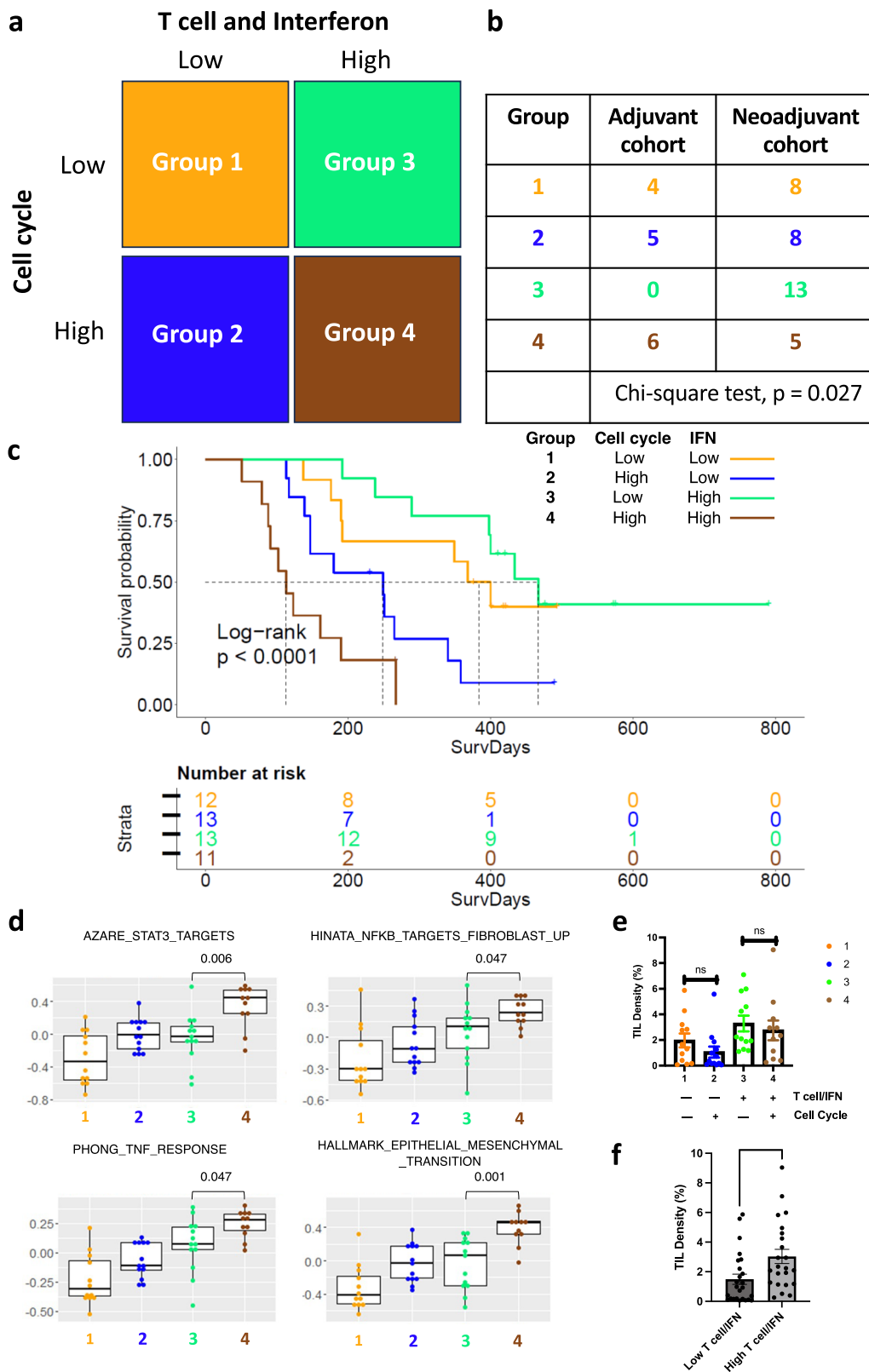
Bulk RNAseq

Paired-end, 2 × 100 base pair (bp) transcriptome reads were mapped to the Genome Reference Consortium Human Build 38 (GRCh38) reference genome using HISAT2 (version 2.0.6) (PMID: 25751142). The gene-level counts were generated by the HTSeq-count program (version 0.5.4p5)[33]. To calculate single-sample gene set enrichment, we used the Gene Set Variation Analysis (GSVA) package (version 1.32.0)[34]. To compute the GSVA scores, the filtered, log2 normalized gene expression were supplied to the GSVA program using the 'kcdf=Gaussian' mode. We manually selected gene sets from the c2.cgp, c6, c7, hallmark geneset collections of the Broad Institute's Molecular Signatures Database (version 7.0)[35]. We utilized CIBERSORTx (https://cibersortx.

Fig. 3 | Cell cycle/cancer proliferation and T cell and interferon signatures define survival groups in patients treated with neoadjuvant pembrolizumab. **a** Participants were classified on the basis of their cell cycle/cancer proliferation and T cell/interferon-γ-related gene signatures into 4 groups. Gene signature high/low was defined as having gene signature enrichment scores above or below the median, respectively **b** Distribution of patients in the neoadjuvant arm versus the adjuvant arm of our clinical trial into the 4 groups defined in (**a**). There was statistically significant uneven distribution of patients among the 4 groups, with all patients in Group 3 coming from the neoadjuvant cohort ($p = 0.027$, Chi-square test). **c** Kaplan–Meier plot of overall survival by group as defined in **a** ($p = 2.77 \times 10^{-6}$, log-rank test). **d** Boxplots for gene signature scores for STAT3 and TNF-α signaling GSEA sets in groups 1-4 ($n = 49$). Each dot represents a patient sample. Middle box line depicts the median, while lower and upper box bounds represent the 25% and

75th percentiles, respectively. Vertical line between data points represents the data range. P values calculated using a Wilconxon rank-sum test. **e** Scatter dot plot of tumor-infiltrating lymphocyte (TIL) density expressed as a percentage of total nucleated cells and stratified by T cell/interferon and cell cycle gene expression signature groups as defined in **a** ($n = 12$; $n = 13$; $n = 12$; $n = 11$ for groups 1–4, respectively). Line is at mean TIL density with error bars denoting the standard error of the mean (n.s. not significant, two-tailed unpaired non-parametric test, Mann–Whitney). **f** Scatter dot plot of tumor-infiltrating lymphocyte (TIL) density expressed as a percentage of total nucleated cells and stratified T cell/interferon gene expression signature alone ($n = 25$ for low T cell/IFN, $n = 23$ for high T cell/IFN). Line is at mean TIL density with error bars denoting the standard error of the mean ($p = 0.0032$, two-tailed unpaired non-parametric test, Mann–Whitney). Source data are provided as a Source Data file.

stanford.edu/) to conduct cell type decomposition on the bulk-RNA-seq data using scRNAseq reference, with the parameters --single_cell TRUE --rmbatchBmode TRUE. The GBM single-cell reference was generated using scRNA-seq data from the study by Abdelfattah et al. (GEO series GSE182109)[36].

Tumor-infiltrating lymphocytes density estimation
To assess the tumor-infiltrating lymphocyte density, we employed the immunoSEQ Assay (Adaptive Biotechnologies) for formalin-fixed, paraffin-embedded tumor samples. The assay amplifies both the TCRβ CDR3 and selected reference genes, which quantitate the total number of T cells and nucleated cells, respectively. Tumor-infiltrating lymphocyte density is calculated by dividing the total number of T cells by the total number of nucleated cells.

Statistics and reproducibility
Statistical analysis was performed using GraphPad Prism v. 10.1.1, Insight Toolkit program (ITK, 2021, version 5.3.0; https://itk.org/), 3D Slicer program (3D Slicer, 2019, version 4.10.2; https://www.slicer.org/), Robust Brain Extraction program (ROBEX, 2013, version 1.2; https://www.nitrc.org/projects/robex/), ITK-SNAP (ITK-SNAP, version 3.8.0; http://www.itksnap.org/pmwiki/pmwiki.php).

Differences in GSVA scores from bulk RNAseq data were determined using an unpaired *T*-test with unequal variances, specifically the two-sided Welch's t-test. To assess the impact on overall survival or time to progression post-treatment, we employed the log-rank test, with visualization facilitated by the Kaplan–Meier technique using R's survminer package. We further performed multivariable cox proportional hazard (cox PH) regression analysis with HRs (95% CIs) to determine if any of the treatment regimen were significantly predictive of overall survival or time to progression after adjusting for clinical covariates, such as age, gender, MGMT and IDH status. We used a Bonferroni correction to account for multiple comparisons. The association between gene set enrichment score and overall survival or time to progression was analyzed similarly using log-rank (univariate) and Cox PH (multivariate) analyses.

Progression-free survival (time from registration to disease progression per iRANO criteria or death) and overall survival (time from registration to death) were estimated in Prism (v10.1.1) using Kaplan–Meier (non-parametric) survival analysis.

Reporting summary
Further information on research design is available in the Nature Portfolio Reporting Summary linked to this article.

Data availability
The RNA sequencing data generated in this study have been deposited in the Gene Expression Omnibus repository under access code GSE264695 for the expanded dataset and GSE121810 for the initial

dataset (https://www.ncbi.nlm.nih.gov/geo/query/acc.cgi). Source data are provided with this paper.

Code availability
R code is available in packages as described in the manuscript.

References
1. Wen, P. Y. et al. Glioblastoma in adults: a Society for Neuro-Oncology (SNO) and European Society of Neuro-Oncology (EANO) consensus review on current management and future directions. *Neuro Oncol.* **22**, 1073–1113 (2020).
2. Reardon, D. A. et al. OS 10.3 Randomized Phase 3 Study Evaluating the Efficacy and Safety of Nivolumab vs Bevacizumab in Patients with Recurrent Glioblastoma: CheckMate 143. *Neuro Oncol.* **19**, iii21 (2017).
3. Omuro, A. et al. Radiotherapy combined with nivolumab or temozolomide for newly diagnosed glioblastoma with unmethylated MGMT promoter: an international randomized phase III trial. *Neuro Oncol.* https://doi.org/10.1093/neuonc/noac099 (2022).
4. Lim, M. et al. Phase III trial of chemoradiotherapy with temozolomide plus nivolumab or placebo for newly diagnosed glioblastoma with methylated MGMT promoter. *Neuro Oncol.* **24**, 1935–1949 (2022).
5. Tawbi, H. A. et al. Combined nivolumab and ipilimumab in melanoma metastatic to the brain. *N. Engl. J. Med.* **379**, 722–730 (2018).
6. Cloughesy, T. F. et al. Neoadjuvant anti-PD-1 immunotherapy promotes a survival benefit with intratumoral and systemic immune responses in recurrent glioblastoma. *Nat. Med.* **19**, v1 (2019).
7. Lee, A. H. et al. Neoadjuvant PD-1 blockade induces T cell and cDC1 activation but fails to overcome the immunosuppressive tumor associated macrophages in recurrent glioblastoma. *Nat. Commun.* **12**, 6938 (2021).
8. Farmer, P. et al. Identification of molecular apocrine breast tumours by microarray analysis. *Oncogene* **24**, 4660–4671 (2005).
9. Li, G. & Wang, X. Prediction accuracy measures for a nonlinear model and for right-censored time-to-event data. *J. Am. Stat. Assoc.* **114**, 1815–1825 (2019).
10. Ayers, M. et al. IFN-γ–related mRNA profile predicts clinical response to PD-1 blockade. *J. Clin. Investig.* **127**, 2930–2940 (2017).
11. Grivennikov, S. I. & Karin, M. Dangerous liaisons: STAT3 and NF-κB collaboration and crosstalk in cancer. *Cytokine Growth Factor Rev.* **21**, 11–19 (2010).
12. Bhat, K. P. L. et al. The transcriptional coactivator TAZ regulates mesenchymal differentiation in malignant glioma. *Genes Dev.* **25**, 2594–2609 (2011).
13. Carro, M. S. et al. The transcriptional network for mesenchymal transformation of brain tumours. *Nature* **463**, 318–325 (2010).
14. Verhaak, R. G. W. et al. Integrated genomic analysis identifies clinically relevant subtypes of glioblastoma characterized by

abnormalities in PDGFRA, IDH1, EGFR, and NF1. *Cancer Cell* **17**, 98–110 (2010).

15. Higgs, B. W. et al. Interferon gamma messenger RNA signature in tumor biopsies predicts outcomes in patients with non–small cell lung carcinoma or urothelial cancer treated with durvalumab. *Clin. Cancer Res.* **24**, 3857–3866 (2018).

16. Karachaliou, N. et al. Interferon gamma, an important marker of response to immune checkpoint blockade in non-small cell lung cancer and melanoma patients. *Ther. Adv. Méd. Oncol.* **10**, 1758834017749748 (2018).

17. Grasso, C. S. et al. Conserved interferon-γ signaling drives clinical response to immune checkpoint blockade therapy in melanoma. *Cancer Cell* **38**, 500–515.e3 (2020).

18. Li, W. et al. Comparison of the regulation of β-catenin signaling by type I, type II and type III interferons in hepatocellular carcinoma cells. *PLoS ONE* **7**, e47040 (2012).

19. Gao, Y. et al. IFN-γ-mediated inhibition of lung cancer correlates with PD-L1 expression and is regulated by PI3K-AKT signaling. *Int. J. Cancer* **143**, 931–943 (2018).

20. Brennan, C. W. et al. The somatic genomic landscape of glioblastoma. *Cell* **155**, 462–477 (2013).

21. Benci, J. L. et al. Opposing functions of interferon coordinate adaptive and innate immune responses to cancer immune checkpoint blockade. *Cell* **178**, 933–948.e14 (2019).

22. Toker, J. et al. Clinical importance of the lncRNA NEAT1 in cancer patients treated with immune checkpoint inhibitors. *Clin. Cancer Res.* **29**, 2226–2238 (2023).

23. Ling, A. L. et al. Clinical trial links oncolytic immunoactivation to survival in glioblastoma. *Nature* **623**, 157–166 (2023).

24. Mineo, M. et al. Tumor interferon signaling is regulated by a lncRNA INCR1 transcribed from the PD-L1 Locus. *Mol. Cell* **78**, 1207–1223.e8 (2020).

25. Deng, J. et al. CDK4/6 inhibition augments antitumor immunity by enhancing T-cell activation. *Cancer Discov.* **8**, 216–233 (2018).

26. Goel, S. et al. CDK4/6 inhibition triggers anti-tumour immunity. *Nature* **548**, 471–475 (2017).

27. Schaer, D. A. et al. The CDK4/6 inhibitor abemaciclib induces a T cell inflamed tumor microenvironment and enhances the efficacy of PD-L1 checkpoint blockade. *Cell Rep.* **22**, 2978–2994 (2018).

28. Zhang, J. et al. Cyclin D-CDK4 kinase destabilizes PD-L1 via cullin 3-SPOP to control cancer immune surveillance. *Nature* **553**, 91–95 (2018).

29. Jerby-Arnon, L. et al. A Cancer Cell Program Promotes T Cell Exclusion and Resistance to Checkpoint Blockade. *Cell* **175**, 984–997.e24 (2018).

30. Rugo, H. S. et al. Abemaciclib in combination with pembrolizumab for HR+, HER2− metastatic breast cancer: Phase 1b study. *npj Breast Cancer* **8**, 118 (2022).

31. Patel, S. et al. LBA6 Neoadjuvant versus adjuvant pembrolizumab for resected stage III-IV melanoma (SWOG S1801). *Ann. Oncol.* **33**, S1408 (2022).

32. Versluis, J. M. et al. Survival update of neoadjuvant ipilimumab plus nivolumab in macroscopic stage III melanoma in the OpACIN and OpACIN-neo trials. *Ann. Oncol.* **34**, 420–430 (2023).

33. Anders, S., Pyl, P. T. & Huber, W. HTSeq—a Python framework to work with high-throughput sequencing data. *Bioinformatics* **31**, 166–169 (2015).

34. Hänzelmann, S., Castelo, R. & Guinney, J. GSVA: gene set variation analysis for microarray and RNA-Seq data. *BMC Bioinform*. **14**, 7–7 (2013).

35. Subramanian, A. et al. Gene set enrichment analysis: a knowledge-based approach for interpreting genome-wide expression profiles. *Proc. Natl Acad. Sci. USA* **102**, 15545–15550 (2005).

36. Abdelfattah, N. et al. Single-cell analysis of human glioma and immune cells identifies S100A4 as an immunotherapy target. *Nat. Commun.* **13**, 767 (2022).

Author contributions

P.Y.W. and T.F.C. designed and co-led this clinical trial. J.R.M.F., E.Q.L., L.N., U.C., R.B., T.T.B., E.A.C., R.G.E., L.D., J.S., K.P., A.S., A.M., C.W., A.R., M.L., A.S., C.L.R., R.G.F, C.M., W.L.B., O.A., P.P.P., G.R.C. K.I.L., I.A.R., J.L.C., D.A.R enrolled clinical trial subjects, provided direct patient care to trial subjects and/or collected patient and tumor data. J.R.M.F., L.S., P.Y.W., R.M.P., T.F.C., G.L. and J.K. designed the analysis plan and analyzed and interpreted clinical and molecular data. J.M.R.F., G.C.Y. and R.H. analyzed neuroimaging data. Manuscript preparation was led by J.R.M.F., L.S., P.Y.W., R.M.P. and T.F.C. All authors contributed to manuscript preparation and revision.

Competing interests

The authors declare the following competing interests: P.P. is the founder and owns equity of Ternalys Therapeutics, inventor of US Patent 11946064 related to non-coding RNA technology. T.F.C. is cofounder, major stock holder, consultant and board member of Katmai Pharmaceuticals, holds stock for Erasca, member of the board and paid consultant for the 501c3 Global Coalition for Adaptive Research, holds stock in Chimerix and receives milestone payments and possible future royalties, member of the scientific advisory board for Break Through Cancer, member of the scientific advisory board for Cure Brain Cancer Foundation, has provided paid consulting services to Third Rock, Symbio, Mundipharma, Tango BlueRock, Vida Ventures, Lista Therapeutics, Stemline, Novartis, Roche, Sonalasense, Sagimet, Clinical Care Options, Ideology Health, Servier, Jubilant, Immvira, Gan & Lee, BrainStorm, Katmai, Sapience, Inovio, Vigeo Therapeutics, DNATrix, Tyme, SDP, Kintara, Bayer, Merck, Boehinger Ingelheim, VBL, Amgen, Kiyatec, Bayer, Abbvie, VBI, Deciphera, VBL, Agios, Novocure, Medscape and has contracts with UCLA for the Brain Tumor Program with Servier, Roche, VBI, Merck, Novartis, BMS, In8bio. The Regents of the University of California (T.F.C. employer) has licensed intellectual property co-invented by TFC to Katmai Pharmaceuticals. P.W. receives research support from Astra Zeneca, Black Diamond, Bristol Meyers Squibb, Chimerix, Eli Lily, Erasca, Global Coalition For Adaptive Research, Kazia, MediciNova, Merck, Novartis, Quadriga, Servier, VBI Vaccines; is a Advisory Board/Consultant to Anheart, Astra Zeneca, Black Diamond, Celularity, Day One Bio, Genenta, Glaxo Smith Kline, Kintara, Merck, Mundipharma, Novartis, Novocure, Sapience, Servier, Symbio, Tango, Telix. R.B. receives funding from Novartis; is a consultant for Scorpion Therapeutics. R.P. receives research support from Merck. The remaining authors declare no competing interests.

Additional information

J. Ricardo McFaline-Figueroa [1,2,15], Lu Sun [3,15], Gilbert C. Youssef[1,4], Raymond Huang[5], Gang Li[6], Jiyoon Kim[6],
Eudocia Q. Lee[1,4], Lakshmi Nayak[1,4], Ugonma Chukwueke[1,4], Rameen Beroukhim [1], Tracy T. Batchelor[1,4],
E. Antonio Chiocca [7], Richard G. Everson [3,8], Lisa Doherty[1], Jennifer Stefanik[1], Kathryn Partridge[1], Amanda Spearman[1],
Alexa Myers[1], Catharina Westergaard[1], Alyssa Russ [1], Maria Lavallee[1], Anna Smokovich[1], Corey LaForest-Roys[1],
Rachel Garcia Fox[1], Christine McCluskey[1], Wenya Linda Bi[7], Omar Arnaout[7], PierPaolo Peruzzi [7], G. Rees Cosgrove[7],
Keith L. Ligon [9], Isabel Arrillaga-Romany[10], Jennifer L. Clarke [11], David A. Reardon [1], Timothy F. Cloughesy [8,12,13,16],
Robert M. Prins [3,8,13,14,16] & Patrick Y. Wen [1,4,16] ✉

¹Center for Neuro-Oncology, Dana-Farber Cancer Institute, Boston, MA, USA. ²Brain & Spine Tumor Center, Perlmutter Cancer Center, NYU Langone Health,
New York, NY, USA. ³Department of Neurosurgery, University of California Los Angeles, Los Angeles, CA, USA. ⁴Department of Neurology, Brigham and
Women's Hospital, Harvard Medical School, Boston, MA, USA. ⁵Department of Radiology, Brigham and Women's Hospital, Harvard Medical School, Boston,
MA, USA. ⁶Department of Biostatistics, Jonathan and Karin Fielding School of Public Health, University of California Los Angeles, Los Angeles, CA, USA.
⁷Department of Neurosurgery, Brigham and Women's Hospital, Harvard Medical School, Boston, MA, USA. ⁸Jonsson Comprehensive Cancer Center, Uni-
versity of California Los Angeles, Los Angeles, CA, USA. ⁹Division of Neuropathology, Brigham and Women's Hospital, Harvard Medical School, Boston,
MA, USA. ¹⁰Division of Neuro-Oncology, Mass General Cancer Center, Harvard Medical School, Boston, MA, USA. ¹¹Departments of Neurology and Neuro-
logical Surgery, University of California San Francisco, San Francisco, CA, USA. ¹²Department of Neurology, David Geffen School of Medicine, University of
California Los Angeles, Los Angeles, CA, USA. ¹³Department of Medical and Molecular Pharmacology, David Geffen School of Medicine, University of
California Los Angeles, Los Angeles, CA, USA. ¹⁴Parker Institute for Cancer Immunotherapy, San Francisco, CA, USA. ¹⁵These authors contributed equally: J.
Ricardo McFaline-Figueroa, Lu Sun. ¹⁶These authors jointly supervised this work: Timothy F. Cloughesy, Robert M. Prins, Patrick Y. Wen.
✉e-mail: Patrick_Wen@dfci.harvard.edu